Current Research in Structural Biology 3 (2021) 121–132

Contents lists available at ScienceDirect

Current Research in Structural Biology

journal homepage: www.journals.elsevier.com/current-research-in-structural-biology

Calmodulin complexes with brain and muscle creatine kinase peptides

Janina Sprenger [a,b,*], Anda Trifan [c,1], Neal Patel [d,1], Ashley Vanderbeck [d], Jenny Bredfelt [a], Emad Tajkhorshid [c], Roger Rowlett [e], Leila Lo Leggio [b], Karin S. Åkerfeldt [d], Sara Linse [a]

[a] Department of Biochemistry and Structural Biology, Chemical Center, PO Box 124, SE-221 00, Lund, Sweden
[b] Chemistry Department, University of Copenhagen, Universitetsparken 5, 2100, Copenhagen, Denmark
[c] Theoretical and Computational Biophysics Group, NIH Center for Macromolecular Modeling and Bioinformatics, Beckman Institute for Advanced Science and Technology, Department of Biochemistry, and Center for Biophysics and Quantitative Biology, University of Illinois at Urbana-Champaign, 405 N Matthews, Urbana, IL, 61801, USA
[d] Department of Chemistry, Haverford College, 370 Lancaster Avenue, Haverford, PA, 19041, USA
[e] Department of Chemistry, Colgate University, 13 Oak Drive, Hamilton, NY, 13346, USA

ARTICLE INFO

Keywords:
Cellular energy metabolism
Calcium signaling
Enzyme regulation
Calmodulin X-ray structure
Isothermal titration calorimetry

ABSTRACT

Calmodulin (CaM) is a ubiquitous Ca^{2+} sensing protein that binds to and modulates numerous target proteins and enzymes during cellular signaling processes. A large number of CaM-target complexes have been identified and structurally characterized, revealing a wide diversity of CaM-binding modes. A newly identified target is creatine kinase (CK), a central enzyme in cellular energy homeostasis. This study reports two high-resolution X-ray structures, determined to 1.24 Å and 1.43 Å resolution, of calmodulin in complex with peptides from human brain and muscle CK, respectively. Both complexes adopt a rare extended binding mode with an observed stoichiometry of 1:2 CaM:peptide, confirmed by isothermal titration calorimetry, suggesting that each CaM domain independently binds one CK peptide in a Ca^{2+}-depended manner. While the overall binding mode is similar between the structures with muscle or brain-type CK peptides, the most significant difference is the opposite binding orientation of the peptides in the N-terminal domain. This may extrapolate into distinct binding modes and regulation of the full-length CK isoforms. The structural insights gained in this study strengthen the link between cellular energy homeostasis and Ca^{2+}-mediated cell signaling and may shed light on ways by which cells can 'fine tune' their energy levels to match the spatial and temporal demands.

1. Introduction

Chemical energy necessary for biochemical processes in all cells is largely provided by adenosine triphosphate (ATP). ATP is primarily produced by oxidative phosphorylation in the mitochondria from where it can be directly exported to the cytosol via diffusion (Elston et al., 1998; Watt et al., 2010; Berg et al., 2010). The energy demand within the cytosol varies spatially and temporally and is regulated through the phosphocreatine energy buffer system (Bessman and Geiger, 1981; Wallimann et al., 1992, 2011). Creatine kinase (CK, EC 2.7.3.2) is particularly important in cells with high-energy consumption, and is expressed as different mitochondrial and cytosolic isoforms, the latter including brain (CKB) and muscle-type (CKM) (Wallimann et al., 2011; Jacobs et al., 1964; Kekelidze and Holtzman, 2003; Bais and Edwards, 1982; Ventura-Clapier et al., 1998). Depending on the substrate concentration, CK converts ATP and creatine (Cr) into creatine-phosphate (CrP) and ADP, or *vice versa* (Bessman and Geiger, 1981). At a high local ATP concentration, the mitochondrial CK isoforms generate CrP, which is exported to the cytosol where at low ATP concentration the cytosolic CK isoforms regenerate ATP and Cr to meet an increased energy demand. This interplay between the mitochondrial and cytosolic CK isoforms is the basis for the cellular ATP shuttle system (Wallimann et al., 2011; Jacobs et al., 1964; Schlattner et al., 2016). Disturbances of this system may cause disease; down-regulation of CKs has been associated with myopathies (Schlattner et al., 2006) and neurodegenerative diseases such as Alzheimer's disease (Kekelidze and Holtzman, 2003; Bais

Abbreviations: ADP, Adenosine diphosphate; ATP, Adenosine triphosphate; Ca^{2+}, Calcium ion (divalent); CaM, Calmodulin; CK, Creatine kinase; CKB, Creatine kinase, brain-type; CKM, Creatine kinase, muscle-type; Cr, Creatine; CrP, Creatine phosphate; Fmoc, Fluorenylmethoxycarbonyl; ITC, Isothermal titration calorimetry; MR, Molecular replacement; PDB, Protein data bank.

* Corresponding author. Center for Free-Electron Laser Science, DESY, Notkestrasse 85, 22607, Hamburg, Germany.
E-mail address: Janina.Sprenger@cfel.de (J. Sprenger).

[1] These authors contributed equally to the study.

https://doi.org/10.1016/j.crstbi.2021.05.001
Received 6 January 2021; Received in revised form 27 April 2021; Accepted 3 May 2021

and Edwards, 1982). It has been suggested that CK further regulates the local ATP concentration through co-localization with energy-consuming enzymes, e.g., with membrane pumps (Schlattner et al., 2016; Wallimann et al., 1984). Though CK plays a major role during drastic changes in ATP demand (Wallimann et al., 2011), its ability to quickly produce the large amounts of ATP needed to fill a temporal energy gap is poorly understood (Hettling and van Beek, 2011).

Cells may experience a temporal 'energy stress' due to the activation of highly energy-consuming processes in response to fast cell signalling (e.g., activation of a muscle cell), which is often mediated through the calcium ion (Ca^{2+}) as a second messenger (Clapham, 1995; Berridge et al., 2000; Bhosale et al., 2015). An incoming signal causes release of Ca^{2+} from intracellular storage compartments to the cytosol and activates calmodulin (CaM) (Chin and Means, 2000). CaM is a universal Ca^{2+}-sensing protein that plays a major role in diverse cellular processes such as signal transduction and muscle contraction (Clapham, 1995; Chin and Means, 2000). The exposure of hydrophobic sites for interaction with target proteins is energetically coupled to Ca^{2+} binding to the EF-hands in CaM. Upon an increase in cytosolic Ca^{2+} concentration, CaM thus binds to and activates several enzymes, including a large number of kinases and membrane pumps (Klee et al., 1986). Such activation of ATP-consuming processes, particularly at cell membranes, causes a temporal energy gap (Wallimann et al., 2011).

It would be beneficial for the cell if ATP regeneration is brought under the same Ca^{2+} control system as the energy consuming activities, i.e. through interaction with CaM. Indeed, in two previous protein-array studies (O'Connell et al., 2010; Herling et al., 2016), more than 100 novel CaM targets were identified, and among them different proteins and enzymes involved in energy metabolism. The current work builds on the discovery of CK from brain, muscle, and mitochondria as CaM target enzymes (Herling et al., 2016). CaM has moreover been shown to increase CKB-catalyzed ATP production 7-fold (Herling et al., 2016) under physiological substrate concentrations (Wallimann et al., 1992), while the cooperativity of substrate binding was abolished by CaM binding (Herling et al., 2016). CKB exists as a homodimer, and in the presence of Ca^{2+}, two CaM have been inferred to bind to two CKB monomers of the dimeric enzyme in a 2:2 stoichiometry (Herling et al., 2016). The newly identified CaM-CK interaction may be important for managing the cellular ATP in a local and temporal manner.

No structural information has yet been obtained for a CaM-CK complex, and the CaM-target site in CK has remained unknown. Structures of the individual proteins, CaM and CK, however, are known. CaM consists of two structurally similar domains (lobes) connected by a linker (Babu et al., 1985, 1988; Finn and Forsén, 1995). Each domain contains two helix-loop-helix Ca^{2+}-binding subdomains referred to as EF-hands, which allow for the binding of up to four Ca^{2+} per CaM (Nakayama and Kretsinger, 1994; Nelson et al., 2002). When cytosolic Ca^{2+} levels increase during signalling processes, the four Ca^{2+} sites of CaM are filled, and CaM undergoes conformational changes to expose hydrophobic patches (Chin and Means, 2000; Klee et al., 1986). In the presence of Ca^{2+}, each lobe exposes a hydrophobic cleft with a significant number of phenylalanine and methionine residues (Babu et al., 1985, 1988; Kretsinger, 1992). As a consequence, the affinity for protein targets, including a range of kinases, is enhanced (Berridge et al., 2000; Tidow and Nissen, 2013; Hoeflich and Ikura, 2002; O'Connell et al., 2013). CaM typically binds to a portion of the target protein that adopts an amphiphilic helix upon binding. There are only a few known cases of crystal structures of CaM in complex with a full-length protein target. Instead, a more tractable approach has been to identify the CaM binding site of the target (Yap et al., 2000), synthesize a target peptide with the respective sequence, and obtain a structure of the CaM-target peptide complex. Structures for many such complexes are available in the protein data bank (PDB), and the structural diversity of CaM in these complexes has been reviewed (Tidow and Nissen, 2013; Hoeflich and Ikura, 2002; O'Connell et al., 2013). The flexibility of the linker joining the N- and C-terminal domains of CaM (N- and C-lobe) allows for a large variation in their relative orientation and binding modes. In the most common binding mode, the peptide is bound by the two CaM lobes in a "hotdog in a bun" manner. There are also examples of complexes of an extended CaM with one or both lobes interacting independently with target peptide (Tidow and Nissen, 2013).

Human CKB and CKM share approximately 80% sequence identity (**SI, Fig. 1**), and their crystal structures are highly similar (**Fig. 1A**) (Bong et al., 2008; Shen et al., 2001). CKM and CKB are both homodimers with each monomer comprising an N-terminal helical domain and a C-terminal α/β domain (residues 1–100 and 125–381, respectively, for CKB), connected by a 24-residue linker (Yap et al., 2000). The loop regions comprising residues 60–70 and 323–332, in the vicinity of the active site, are hypothesized to play an important role in the regulation of the enzyme activity, and their structures differ between isoforms (Bong et al., 2008; Shen et al., 2001; Eder et al., 2008). Structures of CKB in complex with substrates or substrate analogs reveal ligand-dependent structural changes of these loops and the adjacent helices, especially the

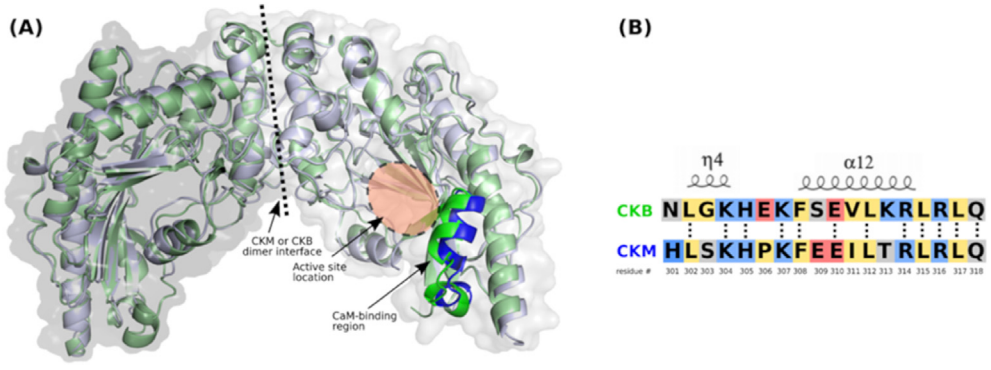

Fig. 1. A,B. CKM and CKB dimer and CaM binding peptides. (A) Overlaid structures of CKB (PDB ID: 3DRE, pale green) with CKM (PDB ID: 1I0E, pale blue) dimers without ligands bound in the active site. The surface is shown in gray. The individual monomers can be distinguished by the different shades of blue/green of the cartoon or silver surface and the dimer interface is indicated by a dotted line. The location of the active site is indicated by an orange oval; the CaM binding peptide of CKB is highlighted in bright green and of CKM in bright blue. (B) The sequence of the CaM-binding peptides with sequence numeration in the peptide and respective CK structure is given. The corresponding secondary structure in the CK structures is indicated above the sequences. The residues are colored according to properties in yellow (hydrophobic), gray (hydrophilic), red (negatively charged) and blue (positively charged). (For interpretation of the references to color in this figure legend, the reader is referred to the Web version of this article.)

amphiphilic helix α12 of the C-terminal region (Fig. 1). Therefore, these loops and helix α12 of that region are possible CaM-binding sites.

In the present study, we have employed X-ray crystallography, isothermal titration calorimetry (ITC), and molecular dynamics (MD) simulations, to study the complex formation between CaM and CK peptides. The results reveal energetic and structural insights into CaM interaction with CKB and CKM. Our findings shed new light on the link between Ca^{2+} signaling and cellular energy metabolism through Ca^{2+}-dependent CaM-CK interactions.

2. Results

2.1. Putative CaM binding peptides from CKB and CKM

The selection of putative CaM-binding regions within CK was based on the identification of amphiphatic helical elements within the human CKB sequence (UniprotID:P12277) using the CaM target data base (Yap et al., 2000) (SI, Fig. 2). combined with manual inspection of the sequence and 3D structure (PDB ID: 3DRE; Fig. 1). Two sequences within CKB were selected and the corresponding peptides synthesized, one covering CKB residues 312–329, i.e., a major part of the structurally mobile loop region at the CKB active site, and one covering CKB residues 301–318 (Fig. 1B), i.e., helix α12 and 3_{10}-turn η4; numbering according to (Eder et al., 2008), as well as part of a loop. The latter is referred to in this study as the CKB peptide. A peptide from CKM covering the region homologous to the CKB peptide (the CKM peptide; residues 301–318; Fig. 1B) was also used to study its binding to CaM.

2.2. ITC studies of peptide binding to CaM and CaM globular domains

The affinity and stoichiometry of binding of each peptide to CaM were evaluated using ITC. Full-length human CaM or individual N- or C-terminal globular CaM domains (N-lobe fragment; C-lobe fragment) were titrated with the peptides from either CKB or CKM in 1.0 mM $CaCl_2$, 10 mM Tris-HCl, 150 mM KCl, pH 7.5. Data obtained with the CKB peptide or the CKM peptide and full-length CaM were best fitted using a 2:1 peptide:CaM stoichiometry. The data were well reproduced using either single average binding constant associated with an average ΔH and or two independent binding constants associated with separate values of ΔH, implying no cooperativity. The two peptides display similar average dissociation constants in the low μM range (CaM:CKB peptide: $K_D = 1.6 \pm 0.3$ μM; CaM:CKM peptide: $K_D = 2.0 \pm 0.2$ μM; Fig. 2). No peptide binding was detected in the absence of Ca^{2+} (i.e., in a buffer with 1.0 mM EDTA), suggesting a strong Ca^{2+} dependence of complex formation. No binding could be detected at any solution conditions for the peptide covering CKB residues 312–329.

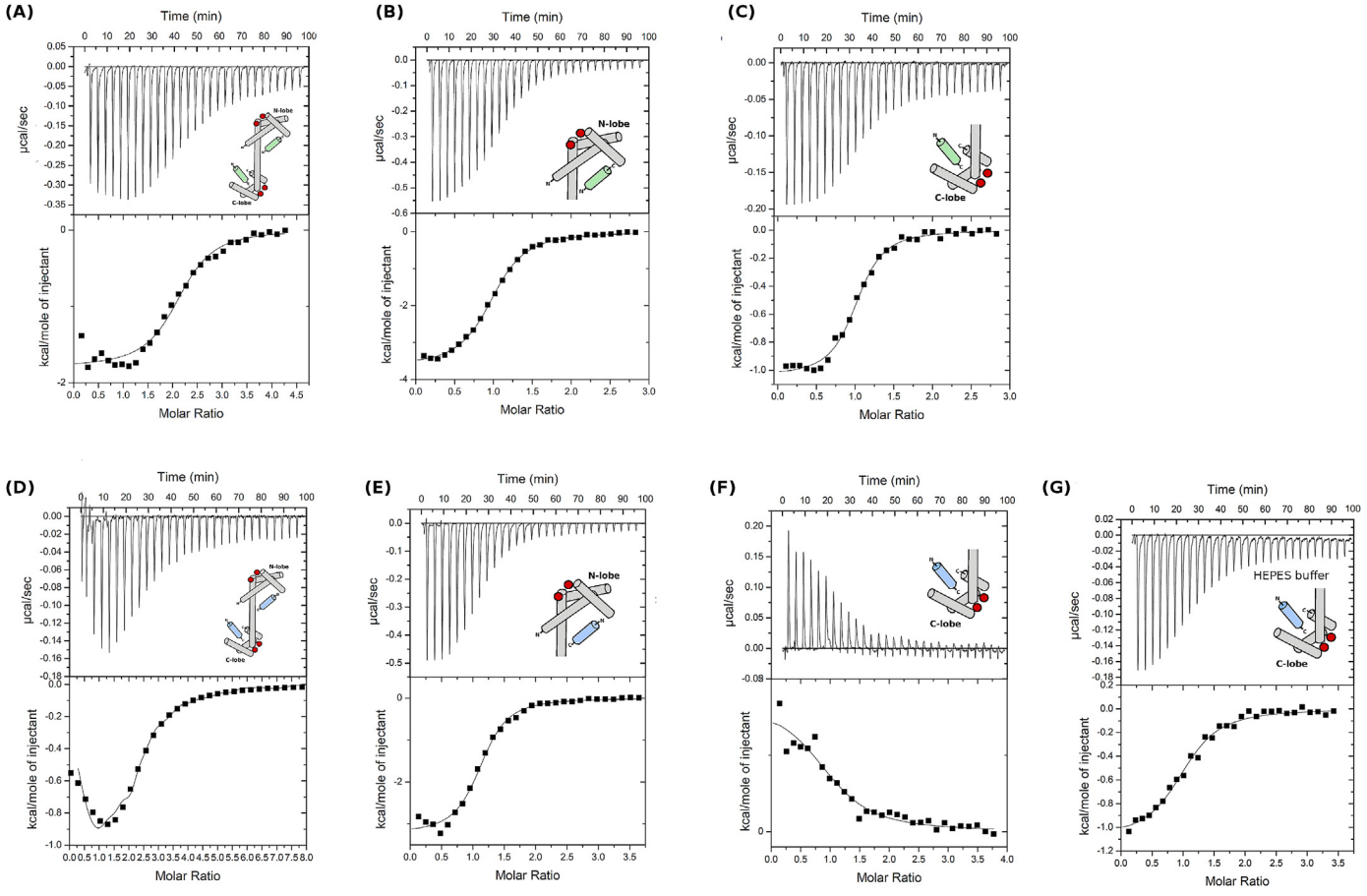

Fig. 2. A–G. ITC of CK peptides with CaM and CaM-lobes. Titration curves for full-length CaM (40 μM) and N- and C-lobe fragments (25 μM) titrated with 500 μM CKB peptide (A–C) and CKM peptide (D–F), respectively, in 10 mM Tris-HCl, 150 mM KCl, 1 mM Ca^{2+}, pH 7.5. The CaM samples and peptides used are indicated by the structural clip-figures. No heat peaks could be detected in buffer with EDTA to keep the free Ca2+ concentration low (Not shown). The titration was done by addition of 10 μM peptide into the cell until saturation and stabilization of the base-line (3–4 molar excess of peptide over CaM-lobe sample and 4.5–8 molar excess of peptide over full length CaM). The titration curves were fitted by a 1:2 binding model (CaM:Peptide) for the titrations of the peptides into the full-length CaM samples and 1:1 for the titrations into the CaM-lobes. The resulting affinities are listed in SI, Table 1. The endothermic signals for the titration of the CKM peptide into the C-lobe of CaM in (F) is due to the large protonation enthalpy of the 10 mM TRIS buffer, while exothermic peaks are obtained in 10 mM HEPES buffer as shown in (G).

The ITC experiments were repeated using the N- and C-lobe fragments, respectively, separately expressed and purified, in 1.0 mM $CaCl_2$, 10 mM Tris-HCl, 150 mM KCl, pH 7.5. The titration data for each fragment with the CKB or CKM peptides (Fig. 2B, C, E, F) are best fit by a 1:1 binding model with a stoichiometry of one peptide per fragment and dissociation constants in the low or sub-μM range. For N-lobe and the CKB peptide: $K_D = 2.0 \pm 0.1$ μM. For C-lobe fragment and the CKB peptide: $K_D = 0.13 \pm 0.02$ μM. For N-lobe and the CKM peptide: $K_D = 1.3 \pm 0.2$ μM. For C-lobe fragment and the CKM peptide: $K_D = 3.6 \pm 0.9$ μM.

Although the aim of the ITC experiments was to estimate the affinity and stoichiometry, we were intrigued by the fact that all experiments in 10 mM Tris, 150 mM KCl, 1.0 mM $CaCl_2$ pH 7.5 revealed an overall exothermic reaction, except for the C-lobe fragment titrated with the CKM peptide in which case an overall endothermic reaction was observed (Fig. 2F; $\Delta H_{tot,T} = 7.1$ kJ/mol). Tris is associated with a large protonation enthalpy, $\Delta H_{p,T} = -47.71$ kJ/mol. The experiment with the C-lobe fragment and the CKM peptide was therefore repeated in 10 mM HEPES 150 mM KCl, 1.0 mM $CaCl_2$ pH 7.5 ($\Delta H_{p,H} = -21.08$ kJ/mol) yielding $\Delta H_{tot,H} = -4.6$ kJ/mol (Fig. 2G). The enthalpy change of the binding reaction, ΔH, and the number of protons transferred per binding event, n, was resolved from the equation system

$$\begin{cases} \Delta H_{tot,T} = \Delta H + n\,\Delta H_{p,T} \\ \Delta H_{tot,H} = \Delta H + n\,\Delta H_{p,H} \end{cases}$$

as $\Delta H = -14$ kJ/mol, and $n = -0.44$. Thus, the binding reaction is indeed exothermic and protons are transferred to the buffer, implying an average increase in pKa values of peptide or protein upon complex formation (Lund and Jönsson, 2005). The dissociation constant for the C-lobe fragment with the CKM peptide is similar in both buffers and the weighted average is $K_D = 3.6 \pm 0.9$ μM. For completeness all resulting values (K_A, K_D, n) from the ITC experiments are summarized in SI, Table 1.

2.3. Crystallization and X-ray diffraction of CaM/CKB-peptide and CaM/CKM-peptide complexes

Crystals of Ca^{2+}-CaM in complex with CKB or CKM peptide, respectively, appeared within 1–2 days as plate clusters (SI, Fig. 3) under the same crystallization conditions (25% PEG 1500, 12.5 mM succinic acid, 44 mM sodium phosphate, 44 mM glycine, pH 4–5). Data sets from separated individual plates were collected with maximum resolutions of 1.24 Å and 1.43 Å for the CaM/CKB-peptide and CaM/CKM-peptide complexes, respectively. The data sets were processed in spacegroup $P2_1$ for the CaM/CKB-peptide and $C2$ for the CaM/CKM-peptide complex (data collection statistics shown in Table 1). The CaM/CKB-peptide structure was solved using molecular replacement (MR), in which the N-terminal CaM domain from the NMR structure of CaM in complex with a binding peptide from calmodulin kinase I (PDB ID: 2L7L, residues 3–79) was used as initial search model in combination with manual placement of the C-terminal CaM domain. This MR solution for the CaM/CKB-peptide complex was then used as a search model to solve the CaM/CKM-peptide structure. The electron density for CaM allowed placement and refinement of residues 3–148 of CaM for the complex structure with CKB peptide and residues 5–147 of CaM in the case of CKM peptide structure. The refinement statistics are shown in Table 1. Both complex structures show two bound peptides, one to each domain of a CaM molecule in an extended conformation (Fig. 3).

The electron density for the peptides (shown in SI, Fig. 4) is generally less defined than for CaM and, except for the CKB peptide bound to the C-lobe, not all peptide residues could be modeled, in particular the position of the first N-terminal residues is largely undefined (described below). The peptide residues building up the amphiphatic helix (residues 308–314; Fig. 1B) could all be assigned and found to adopt the same structure as within the α12 helix of the full-length crystal structures for CKB (PDB ID: 3DRE) and CKM (PDB ID: 1I0E), respectively (Figs. 1 and

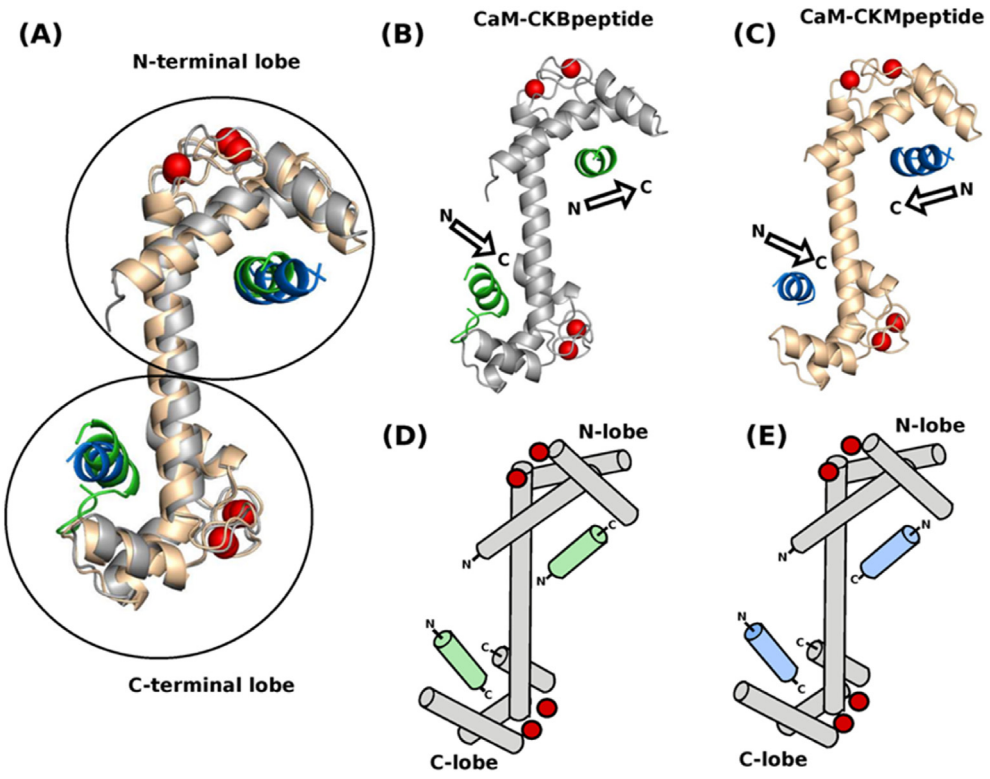

Fig. 3. A–E. CaM/CKB-peptide and CaM/CKM-peptide crystal structures. (A) Overlay of CaM/CKB-peptide peptide structure (gray cartoon with green helical peptides) with CaM/CKM-peptide structure (pale orange cartoon with blue peptides). Structure of CaM/CKB-peptide in same color code as for (A) shown in (B) with indicated direction of the peptide helices by arrows. In analogy the CaM/CKM-peptide structures are shown in (C) with color coding as in (A). Clip figures of the individual structures are shown below the corresponding structures as (D) (CaM/CKB-peptide) and (E) (CaM/CKM-peptide).

Table 1
Crystallographic table.

Complex	CaM/CKB-peptide	CaM/CKM-peptide
Data collection	ESRF ID23-1	ESRF ID30B
PDB code	7BF1	7BF2
Collection statistics		
Resolution range (Å)	39.16–1.23 (1.27–1.24)*	38.87–1.43 (1.48–1.43)
Space group	$P2_1$	$C2$
Unit cell a,b,c (Å)	24.41 59.34 52.48	105.69 24.53 60.35
α,β,γ (°)	90.00 98.34 90	90 104.83 90
Multiplicity	7.2 (7.1)	7.0 (6.2)
Completeness (%)	98.85 (97.65)	97.46 (88.93)
Mean I/sigma (I/σ)	15.76 (1.44)	14.60 (0.96)
Wilson B-factor (Å^2)	16.20	23.40
R-merge	0.048 (1.19)	0.051 (1.50)
R-meas	0.052(1.28)	0.056 (1.65)
$CC_{1/2}$	0.99 (0.60)	0.99 (0.51)
CC*	1 (0.85)	1 (0.82)
Refinement		
R-work (%)	13.5	20.6
R-free (%)	18.6	23.8
RMSZ (bond lengths)	0.71	0.86
RMSZ (angles)	1.04	0.91
Ramach. favored (%)	98.8	99.0
Ramach. allowed (%)	1.2	1.0
Average B-factor (Å^2)	23.0	36.0
Solvent content (%)	24.97	29.91
Number protein residues	146 *(3–148, chain A)*	143 *(5–147, chain A)*
Number peptide molecules	2	2
Number peptide residues	18 *(301–318, chain C)*	15 *(304–318, chain C)*
	11 *(307–317, chain D)*	13 *(306–318, chain D)*
Number waters	148	83

*Numbers in brackets represent statistics for highest resolution shell.

4). Both complexes show a tight crystal packing resulting in a low solvent (water) content of 25% and 30% for the CaM/CKB- and CaM/CKM-peptide complex, respectively. The overall quality of the structures is very good as indicated by the values from refinement statistics and MolProbity scores reported in Table 1. The R_{work}/R_{free} values of both structures are slightly higher compared to other structures with similar resolutions in the PDB. The partial disorder of some of the peptide residues is a likely cause for these slightly elevated values.

2.4. Ca^{2+}-coordination and crystal contacts

All four EF-hands of each structure show full occupancy of four canonical Ca^{2+} binding sites with pentagonal bipyramidal coordination of Ca^{2+} (Fig. 3 and SI, Fig. 5). The Ca^{2+}-coordination is generally highly similar to previously described Ca^{2+}-loaded CaM structures (Babu et al., 1988) in the Ca^{2+}-sites (numbered from N-to C-terminus of CaM) in both complexes. However, some variation is seen in regards to the Ca^{2+}-coordinating water molecule, typically found in EF-hand sites (Babu et al., 1988). The Ca^{2+} in site 1 of both complex structures is instead coordinated by a carboxyl oxygen of Asp119 from a symmetry-related molecule (distance of 3.5 Å to Ca^{2+}; SI, Figs. 5 and 6); this is propagating throughout the entire crystal lattice for both crystal structures despite the different spacegroups, $P2_1$ for the CKB peptide complex and $C2$ for the CKM peptide complex. Some other extended CaM crystal structures display a similar crystal contact interface, e.g. in CaM in complex with peptides from the NADPH oxidase 5 (PDB ID: 6SZ5) (Fañanás et al., 2020), whereas the distance of >4 Å between the carboxyl oxygen of Asp119 and Ca^{2+} is too large for a Ca^{2+}-coordination in some cases (e.g. PDB ID: 6MUE and 1EXT).

2.5. CKB and CKM peptide orientation and contacts in the CaM-lobes

The CKB and CKM peptides are bound to the C-lobe of CaM in a similar orientation (~25° shift between the helix axes; Fig. 3). In the N-lobe, the peptides bind at a similar position, but in reverse orientation (180° rotation) with the N-terminus of one peptide located at the position of the C-terminus of the other peptide (Figs. 3 and 4). Hydrophobic residues within the contact surfaces are listed in Table 2 and shown in SI, Fig. 7. Contacts between polar and charged moieties with distance <4 Å are listed in Table 3 and shown in Fig. 4A.

2.6. Protein-peptide interface in CaM/CKB-peptide complex

The electron density of the CKB peptide bound to the N-lobe allows only residues 307–317 to be reliably modeled (Fig. 4A). The peptide density is much better defined in the C-lobe and allows model building of the entire CKB peptide (residues 301–318; Fig. 4C). The hydrophobic residues of the helical part (α12) of both CKB peptides are facing the hydrophobic groove of each CaM lobe. Analysis of the peptide-CaM interfaces with PISA (Krissinel, 2015) showed that the buried surface area of the peptide and the CaM residues is to a larger extent composed of hydrophobic residues for the N-lobe (~70%) than for the C-lobe (~51–59%) (Fig. 4A), which instead displays a larger number of polar and charged contacts with residues framing the α12 helix (Table 3). Within the peptide bound to the C-lobe, the carboxyl oxygens of Glu310 are in close proximity to both primary amino nitrogen atoms of Arg314. Furthermore, several water molecules are present at the CaM-peptide interfaces, which may hydrogen bond with peptide residues (Fig. 4).

2.7. Protein-peptide interface in CaM/CKM-peptide complex

The CKM peptide electron density is less defined than for the CKB peptides, though at the N-lobe a larger number of residues (304–318) could be identified for the CKM peptide compared to the CKB peptide (Fig. 4B). For the peptide bound to the C-lobe, however, only residues 306–318 were clearly visible (Fig. 1; Fig. 4D and SI, Fig. 3). Contacts between the CKM peptide and CaM residues are primarily between the hydrophobic α12 helix residues and the residues at the hydrophobic pocket in each of the CaM lobe (Table 2; Fig. 4A–D and SI, Fig. 7). The buried surface areas contain a similar high proportion of hydrophobic residues of 70% and 75% (N-lobe), and 74% and 71% (C-lobe), for the peptide and CaM, respectively. The CKM peptide bound to the C-lobe presents more polar contacts compared to the peptide bound to the N-lobe (Table 3). Within the peptide bound to the C-lobe there is a close contact between the side-chain guanidinium group of Arg314 and the backbone carbonyl oxygen of Leu313.

2.8. Computational modeling of CaM binding to CKB

To investigate possible modes of interactions of Ca^{2+}-bound lobes of intact CaM with full-length CKB, we constructed a structural model based on the CaM/CKB-peptide X-ray structures reported here and previously solved X-ray structures of dimeric CKB. In the CaM/CKB-peptide structure, the short CKB peptide is bound to both the C-lobe and the N-lobe of extended CaM, allowing two possible interactions of CaM with the CKB dimer. To take into account the flexibility of the linker between the CaM lobes, a hybrid structure was constructed using a peptide-binding lobe from the CaM-CKB crystal structure plus a flexible loop and the other lobe from an NMR structure as described in the methods. One starting model has the C-lobe (Fig. 5A), and another the N-lobe (Fig. 5B) of CaM bound to the corresponding residues in full-length CKB as found in the CaM/CKB-peptide crystal structure. Each model is composed of the dimeric CKB structure, and the corresponding two full CaM structures bound to each of the two CKB monomers. Both models thus have a stoichiometry of 2:2 (CKB:CaM), based on solution data (Herling et al., 2016). The models were refined using MD simulations with added virtual springs (restraints) between the helix of the CKB monomer and the contacting residues in the CaM lobe according to the CaM-CKB crystal structure (see Methods). The distances used for the virtual springs (harmonic restraints) were obtained from the CaM/CKB-peptide crystal structure in the form of

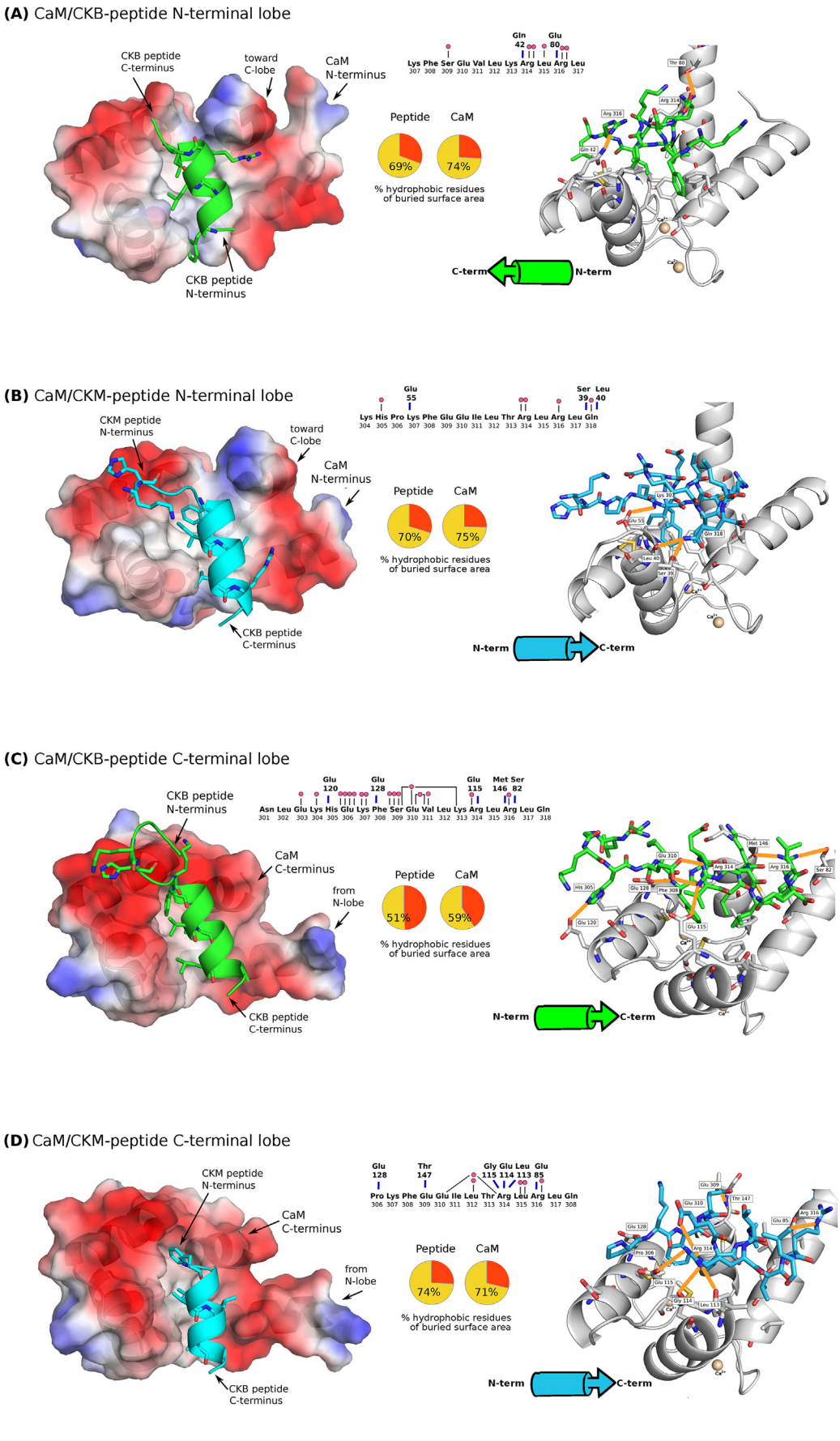

Fig. 4. A–D. Interactions between CaM and the CK peptides. Binding of CKB and CKM peptides to the different CaM lobes: (A) CKB peptide in the N-teminal CaM-lobe, (B) CKM peptide in the N-teminal CaM-lobe, (C) CKB peptide in the C-teminal CaM-lobe, (D) CKM peptide in the C-teminal CaM-lobe. To the left of each, CaM with hydrophobic areas shown in white, surfaces of negatively charged residues shown in red and of positively charged residues in blue. The bound peptide is shown as cartoon in green and blue, for CKB and CKM, respectively, and specific residues are highlighted as sticks to visualize the interface, especially to show fitting of the hydrophobic residues of the peptide into the hydrophobic patch of the CaM-lobe. The pie charts represent the contribution of hydrophobic residues (yellow) and polar residues (red) to the buried surface area. The surface analysis was performed using jsPISA (Krissinel, 2015). Contacts between the peptide residues with waters (pink balls and black lines) or CaM residues (blue lines) including types of atoms interacting are indicated based on the peptide sequence. To the right, the backbone of CaM is shown as cartoon and the bound peptide as sticks with as carbons in green and blue, for CKB and CKM, respectively, oxygen in red, nitrogen in blue and sulphur in yellow. The orientation of the peptide from C-to N-terminus is indicated by a cylinder showing the helix and an arrow pointing to the C-terminus. CaM-residues within a radius of 4 Å around any atom of the bound peptide residue are shown as sticks with carbons in gray, oxygen in red, nitrogen in blue and sulphur in yellow. Contacts of <4 Å distance between atoms of polar amino acids are indicated by orange lines and the residues are labeled.

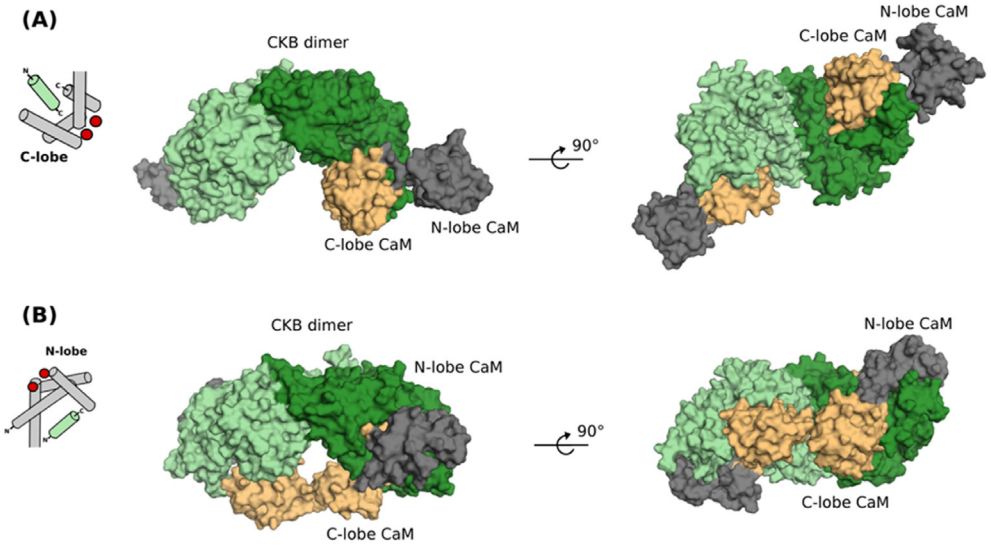

Fig. 5. A,B. CaM-CKB models.
Models of CKB with bound CaM include dimeric CKB based on the ligand-free structure (PDB ID: 3DRE) and a hybrid of the crystal structure of the CaM/CKB-peptide crystal structure (always the lobe that is bound to CKB) and an NMR model (the other lobe) to account for CaM flexibility in solution. The computational models after 250 ns MD simulations are shown in two different orientations in surface representations (green) with (A) CaM C-lobes (orange) or (B) CaM N-lobes (gray) bound to CKB. The tetrameric complexes show a 2:2 binding of 2 CaM bound to 2 CKB that is organized as dimer (the individual monomers are colored in light and dark green).

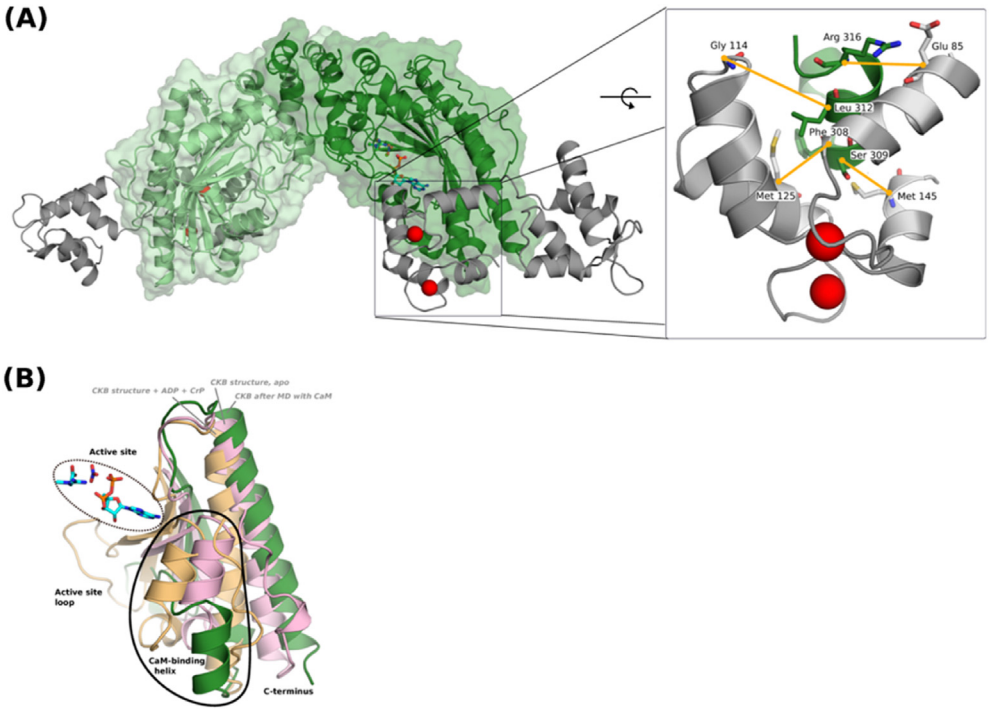

Fig. 6. A,B. CaM-CKB model and active site loop mobility.
The model of two CaM molecules with their C-lobes bound to the CKB dimer (A) as in Fig. 5A but shown as a transparent surface (with one monomer in lighter and the other in darker green) and also including the CKB structure as cartoon. The two CaM molecules are presented as cartoon with Ca^{2+} (in the C-lobe) shown as red spheres. A zoom-in is shown of the CaM-CKB binding site (The model after 250 ns simulation) with EXTRABONDS indicated as orange lines with highlighted residues for the constraints as sticks with carbon in gray or green for the CaM and CKB structures, respectively and oxygen in red, nitrogen blue and sulphur in yellow. The active site region of the C-terminus of CKB (B) is shown for the crystal structures of CKB with bound ADP and CrP (Yellow ribbon, PDB ID:3B6R) without ligand bound (rose ribbon, PDB ID: 3DRE) and after simulation with bound CaM (green ribbon) with CaM binding region is highlighted by a black oval. The active site is shown by the ligands (ADP, CrP and NO_3) as stick models from the ligand bound structure (PDB ID: 3B6R) with carbon in light blue, nitrogen in dark blue, phosphor in orange, and oxygen in red.

four pairs of Cα atoms from CaM and the CKB peptide, respectively, as shown in SI, Fig. 6A and Table 2. To maintain the secondary structure of the peptide, the dihedral angles in the helix were restrained to the values seen in the crystal structure of the CKB dimer (Bong et al., 2008).

After 250 ns of MD simulation of the resulting complexes, the computational models with C-lobe bound to CKB had an RMSD of 1.95 Å and 2.6 Å (calculated with respect to the CaM-CKB peptide crystal structure), respectively, while the N-lobe structure had higher RMSD values of 4.4 Å and 4.8 Å. The higher RMSD values for the N-lobe model may be due to steric clashes in the starting model between CaM and the flexible loop of the C-terminal region of the CKB monomers. The CKB dimers may thus need to significantly alter their structure in order to accommodate the N-lobe, i.e., both proteins may undergo large conformational changes upon complex formation.

3. Discussion

The results of the current ITC and structural studies clearly show that one CaM may interact simultaneously with two CK peptides. The crystal structures of Ca^{2+}-loaded CaM in complex with peptides derived from brain and muscle type CK, show CaM in an extended conformation, binding two identical peptides of either CKB or CKM. All four EF-hands are occupied with Ca^{2+} in a pentagonal bipyramidal fashion, albeit in one site the canonical Ca^{2+}-coordinating water molecule is replaced by an Asp side chain (Asp 119) from an adjacent CaM molecule. This and the extended central helix are likely crystallographic artefacts, but nevertheless we may still discuss here other prominent and potentially biologically relevant features of the structures observed in this study.

ITC reveals binding of the CKB and CKM peptides to CaM in the presence of Ca^{2+}. The stoichiometry (n = 2) agrees with the 2:1

Table 2
Buried hydrophobic residues in the contact zone between CaM and CKB/CKM peptide.

Complex	N-lobe contacts		C-lobe contacts	
	CaM	peptide	CaM	peptide
CaM/CKB-peptide	Leu19	Phe308	Phe93	Phe308
	Phe20	Val311	Leu106	Val311
	Leu33	Leu312	Met125	Leu312
	Val36	Leu315	Phe142	Leu315
	Met37			
	Met52			
	Val56			
	Phe69			
	Met72			
CaM/CKM-peptide	Ala16	Phe308	Ile86	Phe308
	Leu19	Ile311	Ala89	Ile311
	Phe20	Leu315	Val92	Leu315
	Val36		Phe93	
	Met37		Leu106	
	Leu40		Met110	
	Met52		Leu113	
	Ile64		Met125	
			Ala129	

Table 3
Short-range contacts between polar and charged residues in CaM and CKB/CKM peptide.

Complex	N-lobe contacts	C-lobe contacts
CaM/CKB-peptide	Gln42 (NH2): Arg314 (N)	Ser82(OH): Arg316(N)
	Thr80 (OH): Arg314 (N)	Glu115(COO): Arg314(N)
		Glu120(COO): His305(N3)
		Glu128(COO): Phe308(NH)
		Met146(CO): Arg316(N)
CaM/CKM-peptide	Glu55 (COO): Lys307 (N)	Glu85 (COO): Arg316 (N2)
	Ser39 (OH): Gln318 (NH2)	Glu115(COO): Arg314(N)
	Leu40 (CO): Gln318 (NH2)	Thr147 (NH): Glu309 (COO)
		Glu128 (COO): Pro306 (backbone N)
		Gly114 (OH): Arg314 (N)
		Glu115 (COO): Arg314 (N)

N = primary amine nitrogen, N2 = secondary amine nitrogen, NH2 = side chain amide nitrogen, NH = back bone amide nitrogen, N3 = side-chain ring nitrogen, COO = Side chain carboxyl oxygen, CO = backbone carbonyl, OH = side chain hydroxyl oxygen.

peptide:CaM binding observed in the crystal structures. The data are furthermore well fitted without invoking any cooperativity in agreement with none or minor interactions between the N- and C-lobe in the crystal structures. The higher affinity of the CKB peptide for the C-lobe compared to N-lobe coincides with the higher occupancy of the peptide in the C-lobe in the crystal structure.

A broad range of binding modes have been found for CaM in complex with target proteins, revealing considerable structural flexibility of CaM in target engagement (Tidow and Nissen, 2013). The here observed binding mode of CaM in an extended conformation with one peptide bound to each lobe is relatively unique and has only been seen in one previous case, i.e., CaM in complex with two identical peptides from a NADPH oxidase (PDB ID: 6SZ5) (Fañanás et al., 2020). More commonly, crystal structures that show CaM in an extended conformation contain only one bound peptide to the C-lobe of CaM, as exemplified by a peptide from the voltage-gated Na^+ channel NaV1.5 (PDB ID: 4DJC) (Sarhan et al., 2012) and reviewed by Tidow and Nissen (2013). Other examples show the two CaM domains independently binding two different target peptides, e.g., the CaM-regulated NaV1.4 and NaV1.5 channels (Fig. 7B). These have been intensively studied in order to shed light on the underlying mechanism of Ca^{2+}-dependent regulation, and a mechanism was proposed in which each domain is differently affected by Ca^{2+} binding (Yoder et al., 2019). Other examples of extended CaM-peptide structures include CaM in complex with a 62-residue fragment, comprising two α-helices, from the Na^+/H^+ exchanger NHE1, with each helix interacting with a separate CaM-lobe (PDB ID: 2YGG) (Köster et al., 2011). The structure of a complex of CaM bound to a splice variant of the small conductance K^+ channel protein 2 (SK) similarly displays an extended conformation of CaM with a 73-residue fragment bound to both lobes (PDB ID: 3SJQ) (Zhang et al., 2012). This binding mode includes a 2:2 CaM:peptide complex (Zhang et al., 2012).

A notable feature in the structures reported here is the reverse orientation of the CKB and CKM peptides in the N-lobe of CaM, although their affinities are highly similar (K_D values are within a factor of 1.5), suggesting that there may be a small energetic difference between the two orientations which can be controlled by amino acid substitutions in the CaM-binding region of CK. Six residues differ between the two peptides: Asn301 in CKB *versus* His301 in CKM, Gly303 *vs.* Ser303, Glu306 *vs.* Pro306, Ser309 *vs.* Glu309, Val311 *vs.* Ile311, Lys 313 *vs.* Thr313. Of these substitutions, Glu306 *vs.* Pro306 is the least conservative and may

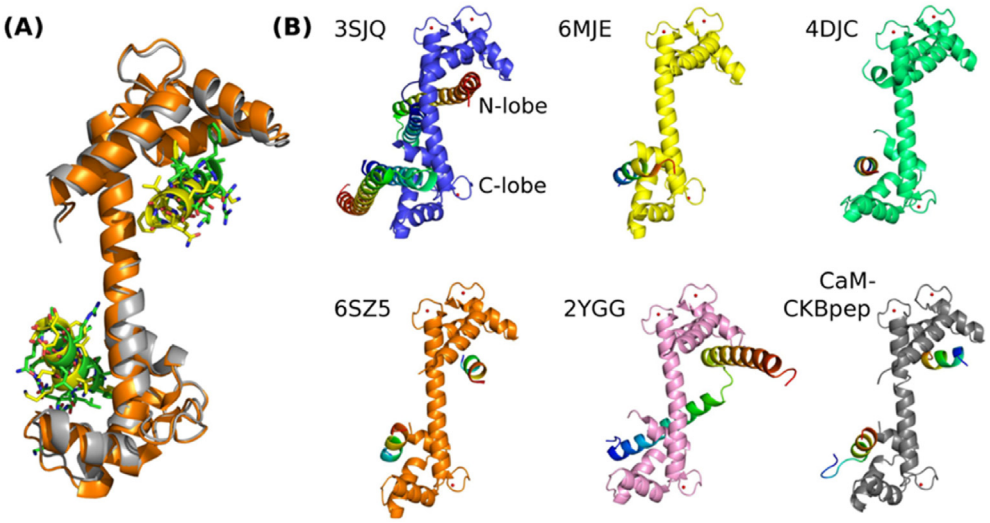

Fig. 7. A,B. Comparison of CaM-peptide structures in extended binding modes. Overlay of structures of CaM with bounds hNOX5 peptide (PDB ID: 6SZ5) with CaM in orange cartoon and peptide in yellow cartoon with sticks and CaM/CKB-peptide with CaM as gray cartoon and peptide in green cartoon with sticks (A). Examples of various extended Ca^{2+}-CaM structures in extended conformation with bound peptides. CaM is represented as cartoon and bound calcium as red balls (B): 3SJQ, CaM in complex with a potassium channel splice variant in blue cartoon; 6MUE CaM with peptide from sodium channel NaV 1.4 as yellow cartoon; 4DJC, CaM with peptide of the NaV1.5 in green; 6SZ5, CaM in complex with peptide from NADPH oxidase 5 as orange cartoon; 2YGG, CaM with peptide from Na+/H+ Exchanger Nhe1 as pink cartoon; The gray cartoon represents CaM in complex with CKB peptide. The peptides are shown as cartoon with rainbow colouring from N-terminus (blue) to C-terminus (red).

play a role in the altered peptide binding pattern of the CKM peptide compared to the CKB peptide. The CKM peptide has an extended non-helical segment including Pro306, which displays contacts with the N-lobe of CaM not observed in the CaM/CKB-peptide structure. Intriguingly, the CaM-binding segments of CKM and CKB (67% sequence identity) are less conserved than intact CK (80% sequence identity). This is also true when comparing CK from different vertebrae (SI, Fig. 1) and may reflect adaptations for differential CaM regulation of CK.

The ITC data and crystal structures provide important information towards understanding the complex formation of CaM with CK and its role in regulation of enzymatic activity. In a previous study, Herling et al. (2016) identified mitochondrial CK, CKM and CKB as CaM targets and characterized the interaction of CaM with CKB, suggesting that one CaM molecule binds each CKB monomer within the CKB dimer (2:2 binding stoichiometry) with a dissociation constant in the low μM range. In this work we find using ITC that one peptide interacts with each lobe and that the affinities in the low μM range are ca. ten-fold higher for the C- relative to N-lobe. This does not necessarily translate to any difference in affinity for the segments in the intact CKB or CKM, and the concentrations used in the crystallization were high enough for both lobes to be occupied by peptide.

The current finding that CaM may interact simultaneously with two CK peptides, i.e., a 1:2 stoichiometry, is not in conflict with the reported 2:2 stoichiometry for intact CaM and CKB in solution (Herling et al., 2016). One resolution would be a model that includes two CaM monomers bound to two CKB monomers in a CK homodimer where only one CaM lobe is involved in binding to the target segment (corresponding to the CKB peptide sequence) in CKB. The results of the MD simulations suggest that binding of the C-lobe to CKB can be achieved with smaller deviations from the starting model (based on PDB ID: 3DRE and this work), compared to the N-lobe. Binding of the N-lobe involves large movements of both CaM and the target segment in CKB, although we cannot exclude the possibility of large conformational changes of the lobes with respect to each other, which is facilitated by the flexible loop connecting them. Based on the observation of the modeling and the ca. 10 times higher affinity of the CKB peptide for the C-lobe compared to the N-lobe, it is possible that two CKB-C-lobe interactions are involved in a 2:2 complex, i.e., two CaM molecules are bound with their C-lobes to one CKB dimer. The modeling further suggests that due to the reverse binding position of the CKM peptide in the N-lobe compared to the CKB peptide, both lobes of CaM may form similar complexes with full length CKM, resembling the C-lobe-CKB complex. In this case, the ITC data show similar affinities of either CaM-lobe for the CKM peptide. Hence, it is possible that CaM binds with either lobe to CKM. It cannot be excluded either that CaM may bridge CKM monomers in separate CKM homodimers, which could lead to polymerization/formation of larger assemblies.

The simulation of the C-lobe/CKB complex (Fig. 5A) suggests that CaM binding likely induces structural changes in the CKB active site; the 301–318 segment is 'pulled away' from the active site (Fig. 6B), which likely affects the adjacent nucleotide binding pocket (Fig. 6B). This is an intriguing observation in the light of the 7-fold increase in ATP production upon Ca_4-CaM binding to CKB at physiological creatine phosphate and ADP concentrations (Herling et al., 2016). The allosterically regulated kinetics of the CK reaction, with a typical sigmoidal response of the activity vs. substrate concentration (Wallimann et al., 2011; Basson et al., 1985), is abolished upon Ca_4-CaM binding, causing increased ATP production within a physiological substrate range (Herling et al., 2016). This mode of regulation is observed for other allosteric enzymes involved in ATP generation, such as phophofructokinase in glycolysis, which switches from a sigmoidal activity at high ATP to a hyperbolic one in the presence of 2,6-bisphosphate or at low ATP concentration (Van Schaftingen et al., 1981). Enzyme activity studies after substitution of residues at the CaM-CK interface may shed light on the molecular determinants of this switch from allosteric CK to an enzyme following classical Michaelis-Menten-type kinetics.

3.1. Concluding remarks

The identification of calmodulin-binding sites in creatine kinase and the high-resolution structures of the complexes between calmodulin and creatine kinase peptides may provide novel insights into the regulation of energy metabolism and its linkage to Ca^{2+} signaling in the cell. Such linkage may stimulate further research with an aim of understanding of how cells overcome the spatial and temporal energy shortages during muscle work and brain activity. The results presented here may also stimulate the development of therapeutic strategies for diseases that originate from altered energy regulation at the cellular level.

4. Materials and methods

4.1. Peptide synthesis

For initial experiments, peptides were made using solid phase methodology employing Fmoc-chemistry (Supplementary methods and materials, SI, 1.1 and 1.2.) of CKB segment with following sequences: AcNH-LKRLRLQKRGTGGVDTAA-CONH2 (CKB residues 312–329, peptide 1) and AcNH-NLGKHEKFSEVLKRLRLQ-$CONH_2$ (CKB residues 301–318, peptide 2). For crystal screening and ITC measurements, the CKB peptide 2 (referred to as CKB peptide) was custom-made and purchased from Genscript including amino-acid analysis for precise analysis of the peptide content of the dried peptide product. Similarily, the homologous peptide sequence of CKB peptide (peptide 2) but from CKM was purchased with the sequence: [AcNH]-HLSKHPKFEEILTRLRLQ-[CONH2] (CKM residues 301–318). For crystallization studies, the CKB and CKM peptides were dissolve to a concentration of 30 mM in MQ water.

4.2. Protein purification

Human wild-type CaM (Uniprot ID: P0DP23, MW 16 828 g/mol) was purified as described in (O'Connell et al., 2010; Waltersson et al., 1993). Prior to crystallization trials, a final size exclusion chromatography step was performed using a Superdex 75 10/300 GL in with buffer containing 10 mM HEPES pH 7 and 5 mM $CaCl_2$. The fractions containing CaM were pooled and concentrated to 20 mg/ml using Amincon Ultra 3K centrifugation devices. The CKB and CKM peptides were dissolved to a concentration of 30 mM in MQ water. The individual CaM domains containing the sequence 1–75 (N-lobe fragment) and 76–146 (C-lobe fragment) were recombinantly expressed in *E. coli* and purified as described previously (Andersson et al., 1983).

4.3. Isothermal titration calorimetry (ITC)

The purified, lyophilized full length CaM or CaM-lobe fragments after gelfiltration with miliQ-water were dissolved in 10 mM TRIS-HCl, 150 mM KCl, pH 7.5 with 1 mM $CaCl_2$ or 1 mM EDTA, or in 10 mM HEPES-KOH, 150 mM KCl, pH 7.5 with 1 mM $CaCl_2$). The CaM-lobe fragments or full-length CaM were introduced into the cell of the ITC instrument (MicoCal VP-ITC) at 40 μM for the individual lobes or 25 μM for CaM. The peptides were dissolved directly into the same buffer as used in the cell, pH checked, and introduced at 500 μM in the syringe. The ITC experiments included 30 additions of 10 μl peptide solution into the cell under constant stirring (300 rpm).

4.4. Crystallization

For crystallization, 10–15 mg/ml CaM in 10 mM HEPES, 5 mM $CaCl_2$ pH 7.0 was incubated for 30 min at room temperature with the CKB peptide in ratios of 1:2, 1:3 and 1:4 CaM:CKB peptide. Initial trials were set up at the crystallization facility in Lund (LP3), Sweden using the commercial screens *Structure 1 + 2, Stura Footprint, PACT premier* and *JCSG+* (all from Molecular Dimensions) in a sitting drop setup and a 1:1

reservoir protein sample ratio with total drop volume of 300 nl. The crystal screens resulted in >40 crystal hits after 2 weeks. All crystals were harvested and tested for diffraction at DESY, Hamburg, beamline P14. The only conditions resulting in protein diffraction (otherwise salt) were 25% PEG 1500, 0.1 M SPG buffer pH 4–5 (from the PACT screen), with CaM:CKB peptide molar ratios 1:3–1:4 (15 mg/ml Ca-CaM). The crystals were reproduced by a 2D hanging-drop grid screen with varying PEG concentrations between 22.5 and 30% with 0.1 M SPG buffer (25% PEG 1500, 12.5 mM succinic acid, 44 mM sodium phosphate, 44 mM glycine) at pH 4 and 5. Crystals grew after 2–3 days as needle or plate clusters for CaM/CKB-peptide ratios of 1:4. These conditions were reproduced also for the complex of CaM with the CKM peptide with same concentrations and CaM:peptide ratios resulting in same crystal forms (needle/plate clusters, as shown in SI, Fig. 3). For either complex the plates and needles with length of 0.05–0.5 mm were separated and soaked for ~30 s in reservoir solution containing 25% glycerol as cryoprotectant before cryo-cooling with liquid N_2 and subsequent data collection.

4.5. Data collection and structure solving

Data sets were collected from single crystals at ESRF, beamline ID23-1 (crystals of CaM/CKB-peptide) and ID30B (crystals of CaM/CKM-peptide). Processing of the datasets was done using XDS (Kabsch, 2010) and autoproc. A resolution cut-off using $CC_{1/2}$ of >0.45 was used (Karplus and Diederichs, 2012). The data were merged and scaled using Aimless (Evans and Murshudov, 2013). The structures were solved by molecular replacement using MOLREP withing the CCP4 package (Vagin and Teplyakov, 2010; Winn et al., 2011). Several deposited structures of full-length CaM with similar cell dimensions have been tested for search (PDB IDs: 1UP4, 4HEX, 4E50, 4DJC, 1CM1) individually but did not provide a successful solution also testing all deposited structures of CaM in the PDB using Mr.BUMP was not successful. A successful solution for the CaM-CKB structure was obtained when using the N-terminal domain of the NMR structure of CaM in complex with a binding from the calmodulin kinase I (PDB ID: 2L7L, residues 3–79) as search model. The initial solution contained two CaM N-teminal domains. One was identified as the C-terminal domain and manually substituted in the electron density (from same search model PDB ID: 2L7L) using the program COOT (Emsley and Cowtan, 2004). After several rounds of restrained refinement with REFMAC5 (Murshudov et al., 2011), additional connected electron density at each lobe was clearly visible as short alpha helix from the peptide. The peptide was built in COOT (Emsley and Cowtan, 2004) by first placing a backbone and also with the help of the corresponding peptide structure in the full-length CKB structure (PDB ID: 3DRE) assigning the peptide residues. The structure was further refined using >100 cycles of restrained refinement including hydrogens with anisotropic B-factor for non-hydrogen atoms in REFMAC5 (Murshudov et al., 2011). The CaM-CKM structure was solved by MR using the CaM structure including Ca^{2+} from the CaM/CKB-peptide complex with removed peptides as search model and manual model building and refinement of the peptide residues as described for the CaM-CKB structure, except that isotropic B-factor refinement was used as anisotropic B-factor refinement did not improve the model or map. Final model validation was done using the validation tool of the PDB.

4.6. Structural modeling

The dimeric CKB structure without active site ligands (PDB ID: 3DRE (Bong et al., 2008)) was generated by choosing symmetry mates that resemble the biological dimer. Missing loops (residues 320–330) from one monomer (chain B) were rebuilt based on chain A using MOE (Molecular Operating Environment (MOE), 2020). The peptide bound to the C-lobe of CaM in the CaM-CK crystal structure was aligned to the corresponding residues in the CKB monomer and placed in an approximate position for binding using VMD (Visual Molecular Dynamics) (Humphrey et al., 1996). These overlaid structures with minimal clashes were taken as a starting point for further modeling using a hybrid crystal-NMR structure for the CaM of the complex to take into account the flexibility of CaM in solution. A common helix from the crystal and NMR structures of the C-terminal lobe of CaM was aligned and a hybrid structure was formed by combining residues 4–73 of CaM NMR structure (PDB ID: 1DMO) (Zhang et al., 1995) and residues 74–148 from the CKB peptide-bound crystal structure for the tentative C-lobe-CKB-peptide bound structure. The procedure was repeated for binding of the N-lobe to CKB and residues 4–74 originating from the CK peptide-bound CaM crystal structure, and residues 75–148 from the NMR structure (PDB ID: 1DMO).

The PSFGEN plugin of VMD (Humphrey et al., 1996) was used to build the protein systems. They were solvated using the SOLVATE plugin of VMD and then neutralized with Na^+ and Cl^- ions for a concentration of 150 mM NaCl using AUTOIONIZE. All simulations were performed using NAMD (Phillips et al., 2005), TIP3P water and CHARMM36 force field for proteins (Best et al., 2012). Langevin thermostat with $\gamma = 0.5\ ps^{-1}$ at 310 K was used. The particle mesh Ewald (PME) method (Essmann et al., 1995) was used to calculate long-range electrostatic forces. A cutoff of 12 Å and a switching distance of 10 Å were used to calculate non-bonded forces. The system was minimized for 3000 steps after which an equilibration of 250 ns for each system was performed during which EXTRABONDS (a feature in NAMD) was used to enforce contacting distances between the helix from CKB and CaM according to the position observed in the CaM-bound crystal structure. An initial spring constant of 0.02 kcal/mol/$Å^2$ was used, which was later increased to 5.0 kcal/mol/$Å^2$. The secondary structure of the CKB helix was kept constant using restraints of 200 kcal/mol/rad (Watt et al., 2010) for the dihedral angles.

Accession numbers

Protein sequences: Human calmodulin (Uniprot ID: P0DP23); Human creatine kinase brain type (Uniprot ID: P12277 sequence 312–329 and sequence 300–318 are used in this study); Human creatine kinase muscle-type (Uniprot ID: P06732; sequence 300–318 is used in this study). *Protein structures:* Calmodulin in complex with a peptide from brain-type creatine kinase, PDB ID: 7BF1; Calmodulin in complex with a peptide from muscle-type creatine kinase, PDB ID: 7BF2.

Funding

The work was supported by funding from the Villum foundation, Denmark (Villum Experiment grant, 17535 to LLL and JS), from the EU ÖKS-interreg project 'Hanseatic League of Science' (HALOS to JS and LLL, grant UCPH-002) and from the Swedish Research Council (2015-00143 to SL). Travel to synchrotrons was supported by the Danish Ministry of Higher Education and Science through the Instrument Center DANSCATT (to LLL). Travel to Lund University (AV and NP) was provided by KINSC, Haverford College, PA, USA. LLL and JS are members of ISBUC, Integrative Structural Biology at the University of Copenhagen (www.isbuc.ku.dk). AT acknowledges support from the United States Department of Energy through the Computational Sciences Graduate Fellowship (DOE CSGF) under grant number:DE-SC0019323. The computational component of the study was supported by the US National Institutes of Health grant P41-GM104601 (to ET).

CRediT authorship contribution statement

Janina Sprenger: Conceptualization, Methodology, Validation, Formal analysis, Investigation, Resources, Writing – original draft, Visualization, Project administration, Funding acquisition. **Anda Trifan:** Methodology, Investigation, Formal analysis, Writing – original draft, Funding acquisition. **Neal Patel:** Investigation, Formal analysis. **Ashley Vanderbeck:** Investigation. **Jenny Bredfelt:** Investigation. **Emad Tajkhorshid:** Supervision, Resources, Writing – review & editing, Funding acquisition. **Roger Rowlett:** Supervision, Validation. **Leila Lo Leggio:**

Validation, Resources, Writing – review & editing, Supervision, Funding acquisition. **Karin S. Åkerfeldt:** Conceptualization, Methodology, Resources, Writing – original draft, Supervision, Project administration, Funding acquisition. **Sara Linse:** Conceptualization, Methodology, Formal analysis, Investigation, Resources, Writing – original draft, Writing – review & editing, Supervision, Project administration, Funding acquisition.

Declaration of competing interest

The authors declare that they have no known competing financial interests or personal relationships that could have appeared to influence the work reported in this paper.

Acknowledgements

We would like to thank the Crystallization facility in Lund (LP3) and especially Dr. Maria Gourdon for experimental guidance. The MX experiments to obtain the CaM-CK peptide complex structure were performed on beamline ID30A-3 at the European Synchrotron Radiation Facility (ESRF), Grenoble, France. We are grateful to Dr. Montserrat Soler-Lopez and Dr. Andrew Mc Carthy at ESRF for providing assistance in using beamline ID23-1 and ID30B, respectively. Initial crystal screening was done at beamlines P13 and P14 operated by EMBL Hamburg at the PETRA III storage ring (DESY, Hamburg, Germany). We would like to thank Dr. Thomas R. Schneider, Dr. Gleb Bourenkov and Dr. Guillaume Pompidor for the assistance in using these beamlines. We furthermore appreciate the scientific discussion with Prof. Jannette Carey, Princeton University, USA.

Appendix A. Supplementary data

Supplementary data to this article can be found online at https://doi.org/10.1016/j.crstbi.2021.05.001.

References

Andersson, A., Forsen, S., Thulin, E., Vogel, J.J., 1983. Cadmium-113 nuclear magnetic resonance studies of proteolytic fragments of calmodulin: assignment of strong and weak cation binding sites. Biochemistry 22, 2309–2313.
Babu, Y.S., Sack, J.S., Greenhough, T.J., Gugg, C.E., Means, A.R., Cook, W.J., 1985. Three-dimensional structure of calmodulin. Nature 315, 37–40.
Babu, Y.S., Bugg, C.E., Cook, W.J., 1988. Structure of calmodulin refined at 2.2 Å resolution. J. Mol. Biol. 204, 191–204.
Bais, R., Edwards, J.B., 1982. Creatine kinase. Crit. Rev. Clin. Lab Sci. 16, 291–335.
Basson, C.T., Grace, A.M., Roberts, R., 1985. Enzyme kinetics of a highly purified mitochondrial creatine kinase in comparison with cytosolic forms. Mol. Cell. Biochem. 67, 151–159.
Berg, J.M., Tymoczko, J.L., Stryer, L., 2010. Biochemistry, seventh ed. W.H. Freeman, New York.
Berridge, M.J., Lipp, P., Bootman, M.D., 2000. The versatility and universality of calcium signalling. Nat. Rev. Mol. Cell Biol. 1, 11–21.
Bessman, S.P., Geiger, P.J., 1981. Transport of energy in muscle: the phosphorylcreatine shuttle. Science 211, 448–452.
Best, R.B., Zhu, X., Shim, J., Lopes, P.E.M., Mittal, J., Feig, M., Mackerell Jr., A.D., 2012. Optimization of the additive CHARMM all-atom protein force field targeting improved sampling of the backbone ϕ, ψ and side-chain χ(1) and χ(2) dihedral angles. J. Chem. Theor. Comput. 8, 3257–3273.
Bhosale, G., Sharpe, J.A., Sundier, S.Y., Duchen, M.R., 2015. Calcium signaling as a mediator of cell energy demand and a trigger to cell death. Ann. N. Y. Acad. Sci. 1350, 107–116.
Bong, S.M., Moon, J.H., Hyun, K., Lee, K.S., Chi, Y.M., Hwang, K.Y., 2008. Structural studies of human brain-type creatine kinase complexed with the ADP–Mg2+–NO3−–creatine transition-state analogue complex. FEBS Lett. 582, 3959–3965.
Chin, D., Means, A.R., 2000. Calmodulin: a prototypical calcium sensor. Trends Cell Biol. 10, 322–328.
Clapham, D.E., 1995. Calcium signaling. Cell 80, 259–268.
Eder, M., Schlattner, U., Becker, A., Wallimann, T., Kabsch, W., Fitz-Wolf, K., 2008. Crystal structure of brain-type creatine kinase at 1.41 Å resolution. Protein Sci. 8, 2258–2269.
Elston, T., Wang, H., Oster, G., 1998. Energy transduction in ATP synthase. Nature 391, 510–513.
Emsley, P., Cowtan, K., 2004. Coot: model-building tools for molecular graphics. Acta Crystallogr. D Biol. Crystallogr. 60, 2126–2132.
Essmann, U., Perera, L., Berkowitz, M.L., 1995. A smooth particle mesh Ewald method. J. Chem. Phys. 103, 8577–8593.
Evans, P.R., Murshudov, G.N., 2013. How good are my data and what is the resolution? Acta Crystallogr. D Biol. Crystallogr. 69, 1204–1214.
Fañanás, E.M., Todesca, S., Sicorello, A., Masino, L., Pompach, P., Magnani, F., Pastore, A., Mattevi, A., 2020. On the mechanism of calcium-dependent activation of NADPH oxidase 5 (NOX5). FEBS J. 287, 2486–2503.
Finn, B.E., Forsén, S., 1995. The evolving model of calmodulin structure, function and activation. Struct. Lond. Engl 3, 7–11, 1993.
Herling, T.W., O'Connell, D.J., Bauer, M.C., Persson, J., Weininger, U., Knowles, T.P.J., Linse, S., 2016. A microfluidic platform for real-time detection and quantification of protein-ligand interactions. Biophys. J. 110, 1957–1966.
Hettling, H., van Beek, J.H., 2011. Analyzing the functional properties of the creatine kinase system with multiscale 'sloppy' modeling. *PLoS Comput. Biol.* Aug 7 (8), e1002130.
Hoeflich, K.P., Ikura, M., 2002. Calmodulin in action: diversity in target recognition and activation mechanisms. Cell 108, 739–742.
Humphrey, W., Dalke, A., Schulten, K., 1996. VMD: visual molecular dynamics. J. Mol. Graph. 14 (33–38), 27–28.
Jacobs, H., Heldt, H.W., Klingenberg, M., 1964. High activity of creatine kinase in mitochondria from muscle and brain and evidence for a separate mitochondrial isoenzyme of creatine kinase. Biochem. Biophys. Res. Commun. 16, 516–521.
Kabsch, W., 2010. XDS. *Acta Crystallogr. D Biol. Crystallogr.* 66, 125–132.
Karplus, P.A., Diederichs, K., 2012. Linking crystallographic model and data quality. Science 336, 1030–1033.
Kekelidze, T., Holtzman, D., 2003. Creatine Kinase and Brain Energy Metabolism: Function and Disease. NATO Science Series: Life and Behavioral Sciences, vol. 342. IOS Press, Amsterdam.
Klee, C.B., Newton, D.L., Ni, W.C., Haiech, J., 1986. Regulation of the calcium signal by calmodulin. Ciba Found. Symp. 122, 162–182.
Köster, S., Pavkov-Keller, T., Kühlbrandt, W., Yildiz, Ö., 2011. Structure of human Na+/H + exchanger NHE1 regulatory region in complex with calmodulin and Ca^{2+}. J. Biol. Chem. 286, 40954–40961.
Kretsinger, R.H., 1992. The linker of calmodulin–to helix or not to helix. Cell Calcium 13, 363–376.
Krissinel, E., 2015. Stock-based detection of protein oligomeric states in jsPISA. Nucleic Acids Res. 43, W314–W319.
Lund, M., Jönsson, B., 2005. On the charge regulation of proteins. Biochemistry 44, 5722–5727.
Molecular Operating Environment (MOE), 2020. 2019.01; chemical computing group ULC, 1010 sherbooke st. West, suite #910, montreal, QC, Canada, H3A 2R7. https://www.chemcomp.com/.
Murshudov, G.N., Skubák, P., Lebedev, A.A., Pannu, N.S., Steiner, R.A., Nicholls, R.A., Winn, M.D., Long, F., Vagin, A.A., 2011. REFMAC5 for the refinement of macromolecular crystal structures. Acta Crystallogr. D Biol. Crystallogr. 67, 355–367.
Nakayama, S., Kretsinger, R.H., 1994. Evolution of the EF-hand family of proteins. Annu. Rev. Biophys. Biomol. Struct. 23, 473–507.
Nelson, M.R., Thulin, E., Fagan, P.A., Forsén, S., Chazin, W.J., 2002. The EF-hand domain: a globally cooperative structural unit. Protein Sci. Publ. Protein Soc. 11, 198–205.
O'Connell, D.J., Bauer, M.C., O'Brien, J., Johnson, W.M., Divizio, C.A., O'Kane, S., Berggård, T., Merino, A., Åkerfeldt, K.S., Linse, S., Cahill, D.J., 2010. Integrated protein array screening and high throughput validation of 70 novel neural calmodulin-binding proteins. Mol. Cell. Proteomics MCP 9, 1118–1132.
O'Connell, D., Bauer, M., Marshall, C.B., Ikura, M., Linse, S., 2013. In: Kretsinger, R.H., Uversky, V.N., Permyakov, E.A. (Eds.), Calmodulin. *Encyclopedia Of Metalloproteins*. Springer, pp. 545–555. https://doi.org/10.1007/978-1-4614-1533-6_67, 2013.
Phillips, J.C., Braun, R., Wang, W., Gumbart, J., Tajkhorshid, E., Villa, E., Chipot, C., Skeel, R.D., Kalé, L., Schulten, K., 2005. Scalable molecular dynamics with NAMD. J. Comput. Chem. 26, 1781–1802.
Sarhan, M.F., Tung, C.-C., Van Petegem, F., Ahern, C.A., 2012. Crystallographic basis for calcium regulation of sodium channels. Proc. Natl. Acad. Sci. U.S.A. 109, 3558–3563.
Schlattner, U., Tokarska-Schlattner, M., Wallimann, T., 2006. Mitochondrial creatine kinase in human health and disease. Biochim. Biophys. Acta BBA - Mol. Basis Dis. 1762, 164–180.
Schlattner, U., Klaus, A., Ramirez Rios, S., Guzun, R., Kay, L., Tokarska-Schlattner, M., 2016. Cellular compartmentation of energy metabolism: creatine kinase microcompartments and recruitment of B-type creatine kinase to specific subcellular sites. Amino Acids 48, 1751–1774.
Shen, Y.Q., Tang, L., Zhou, H.M., Lin, Z.J., 2001. Structure of human muscle creatine kinase. Acta Crystallogr. D Biol. Crystallogr. 57, 1196–1200.
Tidow, H., Nissen, P., 2013. Structural diversity of calmodulin binding to its target sites. FEBS J. 280, 5551–5565.
Vagin, A., Teplyakov, A., 2010. Molecular replacement with MOLREP. Acta Crystallogr. D Biol. Crystallogr. 66, 22–25.
Van Schaftingen, E., Jett, M.F., Hue, L., Hers, H.G., 1981. Control of liver 6-phospho-fructokinase by fructose 2,6-bisphosphate and other effectors. Proc. Natl. Acad. Sci. U.S.A. 78, 3483–3486.
Ventura-Clapier, R., Kuznetsov, A., Veksler, V., Boehm, E., Anflous, K., 1998. Functional coupling of creatine kin a ses in muscles: species and tissue specificity. In: Saks, V.A., Ventura-Clapier, R., Leverve, X., Rossi, A., Rigoulet, M. (Eds.), Bioenergetics of the Cell: Quantitative Aspects, Developments in Molecular and Cellular Biochemistry, vol. 25. Springer, Boston, MA, USA. https://doi.org/10.1007/978-1-4615-5653-4_17.
Wallimann, T., Schlösser, T., Eppenberger, H.M., 1984. Function of M-line-bound creatine kinase as intramyofibrillar ATP regenerator at the receiving end of the phosphorylcreatine shuttle in muscle. J. Biol. Chem. 259, 5238–5246.

Wallimann, T., Wyss, M., Brdiczka, D., Nicolay, K., Eppenberger, H.M., 1992. Intracellular compartmentation, structure and function of creatine kinase isoenzymes in tissues with high and fluctuating energy demands: the 'phosphocreatine circuit' for cellular energy homeostasis. Biochem. J. 281, 21–40.

Wallimann, T., Tokarska-Schlattner, M., Schlattner, U., 2011. The creatine kinase system and pleiotropic effects of creatine. Amino Acids 40, 1271–1296.

Waltersson, Y., Linse, S., Brodin, P., Grundstroem, T., 1993. Mutational effects on the cooperativity of calcium binding in calmodulin. Biochemistry 32, 7866–7871.

Watt, I.N., Montgomery, M.G., Runswick, M.J., Leslie, A.G.W., Walker, J.E., 2010. Bioenergetic cost of making an adenosine triphosphate molecule in animal mitochondria. Proc. Natl. Acad. Sci. U.S.A. 107, 16823–16827.

Winn, M.D., Ballard, C.C., Cowtan, K.D., Dodson, E.J., Emsley, P., Evans, P.R., Keegan, R.M., Krissinel, E.B., Leslie, A.G., McCoy, A., McNicholas, S.J., Murshudov, G.N., Pannu, N.S., Potterton, E.A., Powell, H.R., Read, R.J., Vagin, A., Wilson, K.S., 2011. Overview of the CCP4 suite and current developments. Acta Crystallogr. D Biol. Crystallogr. 67, 235–242.

Yap, K.L., Kim, J., Truong, K., Sherman, M., Yuan, T., Ikura, M., 2000. Calmodulin target database. J. Struct. Funct. Genom. 1, 8–14. http://calcium.uhnres.utoronto.ca/.

Yoder, J.B., Ben-Johny, M., Farinelli, F., Srinivasan, L., Shoemaker, S.R., Tomaselli, G.F., Gabelli, S.B., Amzel, L.M., 2019. Ca^{2+} -dependent regulation of sodium channels Na V 1.4 and Na V 1.5 is controlled by the post-IQ motif. Nat. Commun. 10, 1–12, 2019.

Zhang, M., Tanaka, T., Ikura, M., 1995. Calcium-induced conformational transition revealed by the solution structure of apo calmodulin. Nat. Struct. Biol. 2, 758–767.

Zhang, M., Abrams, C., Wang, L., Gizzi, A., He, L., Lin, R., Chen, Y., Loll, P.L., Pascal, J.M., Zhang, J., 2012. Structural basis for calmodulin as a dynamic calcium sensor. Structure 20, 911–923.